Space-Charge Structural Instabilities and Resonances in High-Intensity Beams

Ingo Hofmann[1,2,*] and Oliver Boine-Frankenheim[1,2]
[1]GSI Helmholtzzentrum für Schwerionenforschung GmbH, Planckstrasse 1, 64291 Darmstadt, Germany
[2]Technische Universität Darmstadt, Schlossgartenstrasse 8, 64289 Darmstadt, Germany
(Received 19 June 2015; published 10 November 2015)

The existence of a structural resonance stop band caused by space charge in high-current beams, where the resonance frequency is associated with 90° phase advance per focusing period, is well known and alternatively referred to in the literature as envelope instability or as fourth-order resonance. We show, however, that this stop band is actually a coincidence of a structural fourth-order resonance and the much stronger envelope instability as competing mechanisms—depending on the time scale and initial matching. A similar complexity of behavior—dependent on the distribution function—is also found between a third-order instability and a sixth-order resonance in a 60° stop band. We claim that these findings are a generic property of high-intensity beams in periodic focusing; they also allow a reinterpretation of the 90° linear accelerator stop band previously observed experimentally at the UNILAC accelerator.

DOI: 10.1103/PhysRevLett.115.204802 PACS numbers: 41.75.Ak, 29.20.Ej, 29.27.Bd

Progress in control of space-charge effects in circular or linear (linac) high-intensity accelerators warrants careful consideration of intrinsic resonant space-charge effects, where space charge itself—combined with linear periodic focusing—is the driving force. Applications are proton drivers for spallation or transmutation facilities or proton or heavy ion injectors for fundamental research.

Frequently cited examples are the envelope instability and the fourth-order resonance in periodic focusing, which are both associated with the "quarter integer" frequency stop band—in linac notation called the "90° phase advance" stop band—where four lattice periods are needed to complete one single-particle oscillation. All physics is described in terms of these phase advances per cell (in degrees per lattice period) without and with space charge, e.g., $k_{0x,y,z}$ and $k_{x,y,z}$, as normalized frequencies. The $k_{x,y,z}$ are understood as uniform beam equivalent values and decreasing with increasing space charge.

The modes discussed here have been introduced in a 2D self-consistent perturbation model of Vlasov's equation for a Kapchinskij-Vladimirskij (KV) distribution in periodic focusing [1]. The first experimental study for coasting beams in a periodic channel with 87 quadrupoles by Tiefenback [2] confirmed noticeable beam degradation for $k_{0x,y} > 90°$. There was evidence for a strong envelope instability, but also for a fourth-order resonance; however, discrepancies with theoretical envelope modeling were large, and an explanation of the difficult measurements remained open.

Subsequently, work on the envelope mode remained theoretical, for example, in Refs. [3–5]. A first experimental test in a linac environment was carried out at the GSI UNILAC high-intensity heavy ion linac [6] in 2009 to clarify whether an envelope instability or a fourth-order resonance driven by space charge dominates as was suggested in Ref. [7]. The experiment, indeed, gave evidence of a fourth-order resonance and not of an envelope instability. However, our findings show that the matter is more complex and warrants revision of the 90° and other relevant stop bands to achieve conceptual clarity on the interplay of the commonly considered *single-particle resonances* (see, for example, Ref. [8]) driven by space-charge "pseudomultipoles" with the less known *resonant space-charge instabilities*.

In uniform density KV beams in a linear periodic lattice, a degradation of emittances can occur only by such resonant instabilities, where the pseudomultipoles grow exponentially from initial noise and lead to emittance growth [1]. Examples studied here are the envelope as well as the third-order instability (60° stop band). It is essential that they equally occur in the non-KV examples, where they cannot be explained by single-particle resonance theory, as their driving terms are absent in matched beams. The fourth- and sixth-order resonances of the 90° and 60°, respectively, stop bands in our simulations, instead, can be in principle regarded as single-particle resonance phenomena, yet with the modification that the space-charge pseudomultipoles are not fixed but self-consistently varying along with the resonance. A fictitious transition from a non-KV to KV beam would transform these resonances into resonant instabilities.

We use the TRACEWIN code [9] and a periodic symmetric focusing-drift-defocusing-drift array of quadrupoles. Longitudinal focusing is by thin rf kicks with k_{0z} chosen as small as 60° to avoid coupling with the $x-y$ motion (k_z typically half of this). Normalized rms emittances are used throughout. They are assumed to be equal initially, which results in bunches slightly elongated from spherical. Note that in the short bunches of linacs the synchrotron period is not very different from betatron periods; in circular accelerators, similar phenomena may occur but modified by

different mixing effects due to the much longer synchrotron periods.

We first employ the (3d) KV-envelope equation option of TRACEWIN thus excluding all effects higher than second order. The envelope instability grows exponentially from infinitesimal mismatch up to saturation by nonlinear space-charge detuning. The full response for $k_{0x,y} = 100°$ and variable $k_{x,y}$ is shown in Fig. 1. $\Delta a/a$ represents the maxima of relative growth taken over 500 cells (usually reached between 50 and 100 cells).

This envelope stop band is only slightly broader than that of the perturbation theory in Ref. [1]—possibly as we are comparing 3d bunches with 2d coasting beams. A necessary criterion for instability is $k_{0x,y} > 90°$ as well as $k_{x,y}$ slightly under 90°, which justifies the nomenclature "90°" stop band. In a recent study of the "120°" stop band of a sixth-order space-charge resonance, the analogous condition $k_{x,y} < 120°$ for resonant growth is explained as a property of the Hamiltonian [10]. The sharp maximum at the right edge, with a very steep drop to zero, is a coherent effect. Entering from the right has a strongly attractive effect: An infinitesimal dilution of space charge causes a corresponding shift of $k_{x,y}$ to the left and induces further growth until $k_{x,y}$ reaches the left edge of the stop band. Entering from the left, instead, pushes $k_{x,y}$ backwards and growth stops.

Next, we apply the TRACEWIN particle-in-cell option to a lattice and bunch identical to Fig. 1; hence, all orders of the bunch space-charge potential act back on particle motion. We start with a Gaussian distribution truncated at 3.4σ. The transverse tune is depressed by space charge to $k_{x,y} = 74°$ ($k_z = 35°$). Emittances along the lattice are shown in Fig. 2 (top). As shown in the insets, an early developing fourth-order space-charge resonance pattern of the kind $4k = 360°$, followed and replaced by the envelope instability of the kind $2k = 180°$, is noteworthy. Here, the notion $n \times k = m \times 360°$ stands symbolically for the respective mode, with n the order of the resonance and m the harmonic of the focusing lattice; it is not to be confused with a resonance condition for single particles. The fourth-order phase space structure evolves immediately, and at cell 15 the ϵ_x, ϵ_y reach a plateau with a factor of 1.7 growth (averaged in x, y). Beam core density and emittance get heavily degraded after about 20 cells, apparently by the steeply rising envelope instability leading to a second plateau with a factor of 4 emittance growth. It is characterized by a dominating twofold symmetry washing out the fourth-order pattern in $x - x'$ (see the inset at cell 35), until decoherence beyond cell 120.

This is confirmed by the so-called "halo" H_x, H_y and "mismatch" M_x, M_y parameters in Fig. 2. The H_x, H_y are defined as ratios of a fourth-order moment to a second-order moment and normalized to zero for uniform density [11]. For a nontruncated Gaussian distribution they are 1, and for a water bag distribution 0.25. The M_x, M_y are related to the deviation from the initial values of the matched envelopes [12]. The results in Fig. 2 indicate a peak of the H_x, H_y at cell 13, where the fourth-order resonance plateau starts. A peak of M_y at cell 30 is followed about 10 cells later by a peak of M_x, which are a clear measure of the envelope growth—accompanied by rising values of the respective emittances. In the envelope instability phase, H_x, H_y drop again and reach, beyond

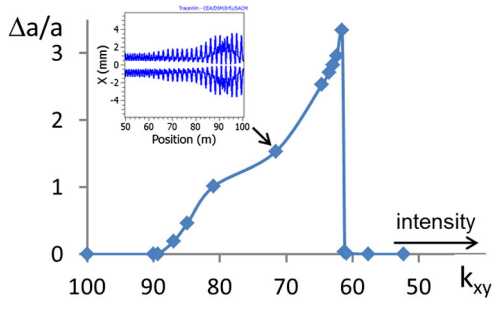

FIG. 1 (color online). Envelope instability resonance stop band showing relative growth of rms envelopes as a function of $k_{x,y}$ (fixed $k_{0x,y} = 100°$). Inset: x envelope from cell 50…100.

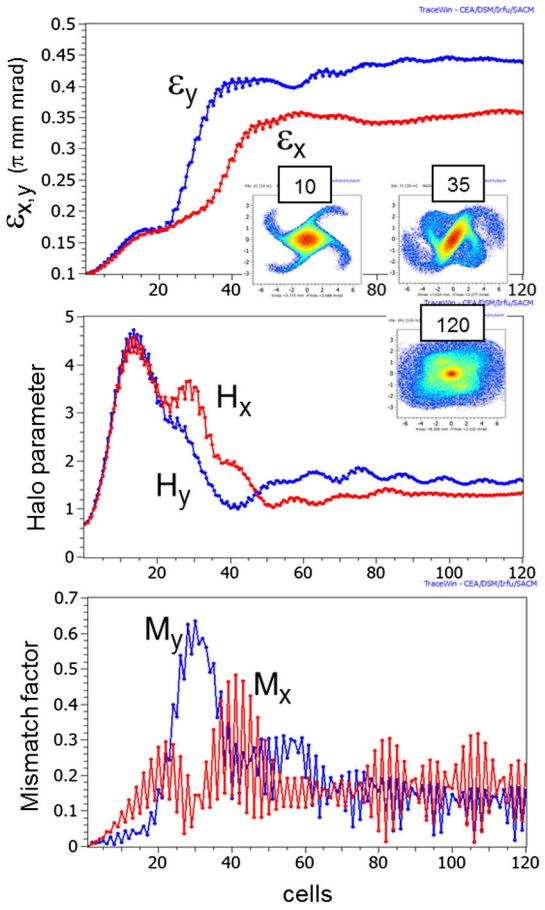

FIG. 2 (color online). Plot of emittances (top, with insets showing $x - x'$ phase space at cells 10, 35, and 120), halo (center), and mismatch parameters (bottom) in x and y as a function of the cell number and for $k_{0x,y} = 100°$.

cell 40, more Gaussian-like values as a result of the beginning decoherence (see inset cell 120). Note that ϵ_x, ϵ_y grow synchronized in the more incoherent fourth-order resonance phase, while their unsynchronized growth beyond cell 40 is typical for an instability situation, where the initial mismatch error matters.

Full response curves after 500 cells for water bag (WB) and Gaussian (G) distributions are shown in Fig. 3, where we have varied $k_{x,y}$ such as to cover a complete stop band analogous to Fig. 1. The distinction between contributions from fourth-order and envelope growth is based on the systematic appearance of the two plateaus shown in Fig. 2 (top), which in all cases are found correlated with the evolution of $M_{x,y}$, $H_{x,y}$ and the characteristic phase space plot symmetries. The first plateau marks the saturation of the fourth-order resonance in the initial phase (fourth/initial); it is followed by the fast-rising envelope instability, which saturates on a second plateau marked as "total," with a significant relative emittance growth up to a factor of 8.

The width and location of the envelope instability response in Fig. 3 are in excellent agreement with the envelope result of Fig. 1. The amount of emittance change also compares well with the envelope change by noting the quadratic dependence of emittance change on mismatch [13]. Remarkably, this applies to both the Gaussian *and* water bag distributions. Note that the vanishing fourth-order response for $k_{x,y} < 74°$ in the water bag case is due to the missing tails in this distribution. The smaller width and the location of the stop band center closer to $k_{x,y} = 90°$—compared with the envelope instability—are roughly consistent with the perturbational fourth-order instability stop bands of the KV distribution in Ref. [1]. As before, resonant growth requires $k_{0x,y} > 90°$ and $k_{x,y} < 90°$. For completeness, we note that beyond the sharply falling right-hand side edge there is an ongoing fourth-order resonance effect, where the values reached at cell 500 are marked in Fig. 3.

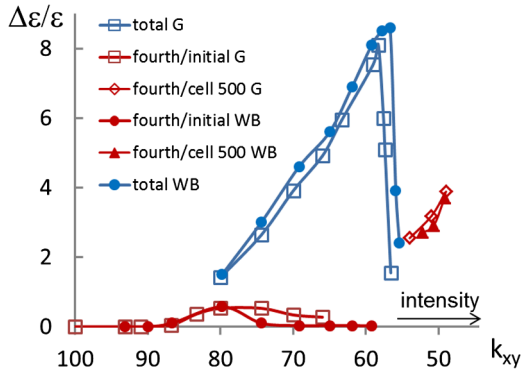

FIG. 3 (color online). Stop bands of structural 90° response for the water bag and Gaussian distributions and fixed $k_{0x,y} = 100°$, showing relative emittance growth versus $k_{x,y}$.

We compare our findings with the UNILAC experiment [6]. The data were taken over 16 cells of the first tank of the Alvarez drift tube linac, with clear evidence of a fourth-order structure in phase space accompanied by 30% rms emittance growth well supported by the simulation. The peak of the response was found near $k_{0x,y} = 100°$, where $k_x = 81.1°$ and $k_y = 84.6°$. Comparison with Fig. 2 as well as Fig. 3 suggests that the experimental data taken at cell 16 fall well inside the "initial fourth-order" regime, which lasts at least up to cell 40 for well-matched beams. The experimental $k_{x,y}$ just above 80° is, however, at the left edge of the envelope instability stop band of Fig. 3. We have carried out simulations for varying $k_{0x,y}$ and fixed current and found that the working point moves into the interior of the envelope stop band and reaches the maximum emittance growth of over 400% approximately at $k_{0x,y} = 95°$. For $k_{0x,y} \to 95°$ the experimental data show, instead, vanishing growth consistent with the fourth-order stop band. Obviously, the experiment would have had to go beyond a length of 30–40 cells to show the much stronger envelope instability. However, we have also found that the initial mismatch plays a significant role. While the average mismatch (in x and y) of the experiment was around 10%, we have found by simulation that doubling this value would have had the effect—even over the length of 16 cells—that the envelope instability appears much earlier, overtaking the fourth-order resonance and roughly doubling the rms emittances. In summary, the earlier conclusion that "this fourth-order resonance is dominating over the better known envelope instability and practically replacing it" [7] is justified only under the special double assumption of short distance propagation *and* good initial matching—otherwise, the much stronger and faster envelope instability takes over. Whether or not good matching combined with fast crossing—within a few cells—offers options to overcome this stop band needs to be checked in concrete designs.

We examine if a similar phenomenon exists at even higher order. For $k_{0x,y} > 60°$, Ref. [1] suggests the existence of a third-order $3k = 180°$ type of instability on the KV-perturbational level. The associated driving terms would be a third-order "pseudosextupole" term (for example, x^3) in the space-charge potential, which is absent in a beam symmetric in x and y. Yet such unsymmetric terms may exist on the noise level, and instability could make them finite. The corresponding eigenmode oscillates with $3k_{0x,y}$ in the absence of space charge, but with space charge its phase advance can get locked to 180° per cell, in which case exponential instability analogous to the envelope instability would be expected. Reference [1] also suggests a sixth-order $6k = 360°$ resonance driven by a "pseudo-dodecapole" component naturally present in a water bag or Gaussian initial distribution.

Using a water bag distribution and examining a case with $k_{0x,y} = 90°$, $k_{x,y} = 42°$ (well inside the third-order stop

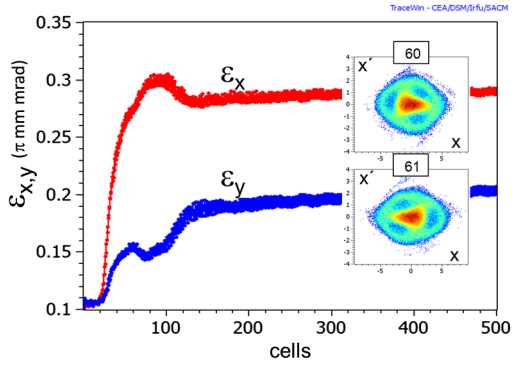

FIG. 4 (color online). Simulation of a water bag distribution with $k_{0x,y} = 90°$, $k_{x,y} = 42°$ showing $x - x'$ phase space plots at cells 60 and 61 and rms emittance evolution.

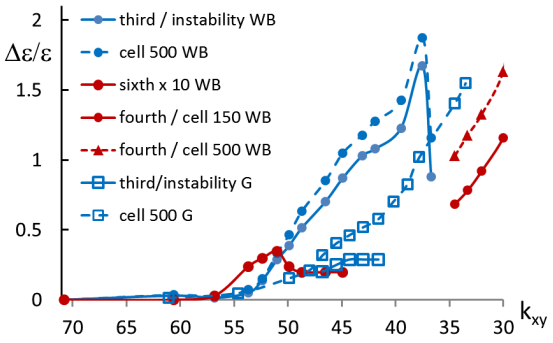

FIG. 5 (color online). Stop bands of structural 60° response for a water bag compared with a Gauss distribution for fixed $k_{0x,y} = 90°$ (sixth order enhanced by a factor of 10).

band characterized in Ref. [1]), we find clear evidence of an exponentially rising third-order mode as shown in Fig. 4. The $x - x'$ phase space pictures at cells 60 and 61 confirm the third-order (triangular) structure, which flips by 180° from cell to cell and requires two cells for a complete period; hence, a parametric instability of the kind $3k = 180°$ is confirmed. The exponential growth is supported by the fast-rising emittance starting shortly after cell 20, where the unsymmetric growth in x and y is again a characteristic of the exponential instability.

The 60° stop band for a water bag distribution shows a maximum of 170% rms emittance increase at 37° by the third-order instability, beyond which it drops sharply as shown in Fig. 5. In addition, we retrieve a $6k = 360°$ resonance with sixfold symmetry phase space structure up to 3.5% rms emittance growth at the low-intensity (left) side of the stop band. Besides this, phase space pictures (with 180° phase advance per cell) support the existence of a fourth-order $4k = 180°$ mode for $k_{x,y} < 35°$. This is also found in Ref. [1], where at $k_{0x,y} = 90°$ a fourth-order 45° perturbation stop band is indicated for $40° > k_{x,y} > 25°$. While these processes all occur relatively early—typically within the first 150 cells—a lower gradient and more incoherent type of resonant growth is ongoing but not clearly associated with third or fourth order (with values at cell 500 indicated in Fig. 5). For comparison, Fig. 5 shows that the Gaussian distribution function has a much weaker indication of this third-order instability and limited to a smaller range of $k_{x,y}$. Instead, there is primarily a more ongoing incoherent resonant response—again not clear of which order—and increasing with space charge. It must be assumed that the additional tails of the Gaussian distribution suppress the strong third-order instability response of the water bag case and lead to a more incoherent response. For both the water bag and Gaussian, the region $60° < k_{x,y} < 90°$ (partly shown) is free of emittance growth, which is just starting for $k_{x,y} < 57°$.

In summary, resonant structural space-charge effects show enhanced complexity. In particular, the competition between instability and resonance effects, like $2k = 180°$ with $4k = 360°$ modes at 90° or $3k = 180°$ with $6k = 360°$ modes at a 60° stop band, has been established. Theoretically, this phenomenon might also occur with correspondingly increasing order modes at 45° or 30°, etc., although it might be difficult in realistic linac beam dynamics with changing parameters to practically identify such phenomena. Yet their existence should not be ignored, if in future high-intensity linacs the space-charge limit is further approached.

The competition between instability and resonance is particularly significant in dealing with the 90° linac stop band and interpreting its nature on this new basis. Its relevance to linac design may warrant further experimental efforts, if it becomes desirable to overcome the not always practical design limitation to less than 90°.

The role of Landau damping by tails of the distribution function and with slow synchrotron motion as common to circular accelerators is left to future work.

The authors are grateful for support by D. Uriot regarding functionalities of the TRACEWIN code and for valuable discussions with L. Groening on the UNILAC experiment.

*i.hofmann@gsi.de

[1] I. Hofmann, L. J. Laslett, L. Smith, and I. Haber, Particle Accelerators **13**, 145 (1983).
[2] M. Tiefenback, Ph.D. thesis, Lawrence Berkeley National Laboratory Report No. LBL-22465, 2006.
[3] J. Struckmeier and M. Reiser, Particle Accelerators **14**, 227 (1984).
[4] S. M. Lund and B. Bukh, Phys. Rev. ST Accel. Beams **7**, 024801 (2004).
[5] C. Li and Y. L. Zhao, Phys. Rev. ST Accel. Beams **17**, 124202 (2014).
[6] L. Groening, I. Hofmann, W. Barth, W. Bayer, G. Clemente, L. Dahl, P. Forck, P. Gerhard, M. S. Kaiser, M. Maier, S. Mickat, T. Milosic, S. Yaramyshev, and D. Uriot, Phys. Rev. Lett. **103**, 224801 (2009).

[7] D. Jeon, L. Groening, and G. Franchetti, Phys. Rev. ST Accel. Beams **12**, 054204 (2009).
[8] E. Wilson, Report No. CERN-1995-006.15, 1993.
[9] D. Uriot, http://irfu.cea.fr/Sacm/logiciels/.
[10] D.-O Jeon, K. R. Hwang, J.-H. Jang, H. Jin, and H. Jang, Phys. Rev. Lett. **114**, 184802 (2015).
[11] C. K. Allen and T. P. Wangler, Phys. Rev. ST Accel. Beams **5**, 124202 (2002).
[12] T. P. Wangler, *RF Linear Accelerators*, 2nd ed. (Wiley-VCH, New York, 2008).
[13] M. Reiser, J. Appl. Phys. **70**, 1919 (1991).